AGU PUBLICATIONS

JGR

Journal of Geophysical Research: Oceans

RESEARCH ARTICLE

10.1002/2015JC010829

Key Points:
- Iron limitation enhances carbon export through silica ballasting
- Surface nutrient ratios track spatial variations in iron stress
- Eddy interactions drive spatial variability in phytoplankton iron stress

Correspondence to:
M. A. Brzezinski,
mark.brzezinski@lifesci.ucsb.edu

Citation:
Brzezinski, M. A., J. W. Krause, R. M. Bundy, K. A. Barbeau, P. Franks, R. Goericke, M. R. Landry, and M. R. Stukel (2015), Enhanced silica ballasting from iron stress sustains carbon export in a frontal zone within the California Current, *J. Geophys. Res. Oceans*, *120*, doi:10.1002/2015JC010829.

Received 11 MAR 2015
Accepted 6 JUN 2015
Accepted article online 11 JUN 2015

Enhanced silica ballasting from iron stress sustains carbon export in a frontal zone within the California Current

Mark A. Brzezinski[1], Jeffrey W. Krause[2,3], Randelle M. Bundy[4], Katherine A. Barbeau[4], Peter Franks[4], Ralf Goericke[4], Michael R. Landry[5], and Michael R. Stukel[6]

[1]Marine Science Institute and the Department of Ecology Evolution and Marine Biology, University of California, Santa Barbara, California, USA, [2]Dauphin Island Sea Laboratory, Dauphin Island, Alabama, USA, [3]Department of Marine Sciences, University of South Alabama, Mobile, Alabama, USA, [4]Geosciences Research Division, Scripps Institution of Oceanography, University of California, San Diego, California, USA, [5]Integrative Oceanography Division, Scripps Institution of Oceanography, University of California, San Diego, California, USA, [6]Department of Earth, Ocean, and Atmospheric Science, Florida State University, Tallahassee, Florida, USA

Abstract Nutrient dynamics, phytoplankton rate processes, and export were examined in a frontal region between an anticyclone and a pair of cyclones 120 km off the coast in the southern California Current System (sCCS). Low silicic acid: nitrate ratios (Si:N) and high nitrate to iron ratios (N:Fe) characteristic of Fe-limiting conditions in the sCCS were associated with the northern cyclone and with the transition zone between the cyclones and the anticyclone. Phytoplankton growth in low-Si:N, high-N:Fe waters responded strongly to added Fe, confirming growth limitation by Fe of the diatom-dominated phytoplankton community. Low Si:N waters had low biogenic silica content, intermediate productivity, but high export compared to intermediate Si:N waters indicating increased export efficiency under Fe stress. Biogenic silica and particulate organic carbon (POC) export were both high beneath low Si:N waters with biogenic silica export being especially enhanced. This suggests that relatively high POC export from low Si:N waters was supported by silica ballasting from Fe-limited diatoms. Higher POC export efficiency in low Si:N waters may have been further enhanced by lower rates of organic carbon remineralization due to reduced grazing of more heavily armored diatoms growing under Fe stress. The results imply that Fe stress can enhance carbon export, despite lowering productivity, by driving higher export efficiency.

1. Introduction

Coastal waters off California are known to be a patchwork of iron (Fe)-replete and Fe-limiting waters that affect both phytoplankton growth and regional biogeochemistry [e.g., *Hutchins et al*., 1998; *Bruland et al*., 2001]. This phenomenon has mainly been examined on the continental shelf and slope where bottom topography and sediment composition cause spatial variations in Fe supply. Waters upwelling along the coast become enriched in Fe through interaction with iron-rich, fine-grained bottom sediments, particularly over broad continental shelves. Where the continental shelf is narrow, upwelled waters are rich in macronutrients, but contain low Fe [*Bruland et al*., 2001].

In the California upwelling regions, interactions between circulation, bathymetry, and Fe have the potential to extend the influence of Fe stress well beyond the continental shelf. Wind-driven coastal upwelling is far from uniform, being enhanced around headlands and other topographic features [*Rykaczewski and Checkley*, 2008]. This leads to variations in cross-shelf flows that can carry upwelled waters with elevated phytoplankton biomass tens of kilometers offshore [*Washburn et al*., 1991], extending the geographic influence of low Fe on plankton dynamics. In addition, gradients in wind stress curl offshore and mesoscale features such as fronts and eddies can drive local upwelling away from the shelf [*Rykaczewski and Checkley*, 2008]. Several recent publications have demonstrated that the effects of Fe-limitation on phytoplankton communities can extend well over 100 km offshore, out to the transition zone between coastally upwelled water and the more oligotrophic waters of the California Current, in both the southern [*King and Barbeau*, 2011] and in the central California Current System [*Biller and Bruland*, 2014].

The iron content of upwelled waters affects macronutrient dynamics, productivity, and potentially, carbon export. The water that upwells along the coast of California contains ~20% more silicic acid than nitrate [*Zentara and Kamykowski*, 1977]. As a result, there is ample silicic acid to support complete nitrate consumption by diatoms [average diatom Si:N demand = ~1; *Brzezinski*, 1985], and diatoms typically dominate the initial phytoplankton response to upwelling. However, off California, as in other Fe-limited regions, low Fe relative to macronutrients drives the preferential depletion of silicic acid over nitrate [e.g., *Bruland et al.*, 2001]. At least two mechanisms are involved: physiological and species composition. Physiologically, low Fe impedes nitrogen assimilation in all phytoplankton and enhances silicic acid utilization in some diatoms [*Hutchins and Bruland*, 1998; *Takeda*, 1998], although it may decrease it in others [*Marchetti and Harrison*, 2007]. The impact on cellular N is typically stronger than the effect on cellular Si, so even in species in which Fe lowers cellular Si, cellular Si:N increases [*Marchetti and Harrison*, 2007]. The impact on diatom elemental composition is significant. Whereas nutrient-replete diatoms have a Si:N mole ratio of 1 [*Brzezinski*, 1985], Fe stress can increase this ratio to 4–6 or higher [*Franck et al.*, 2000]. Photosystems and carbon acquisition pathways are also compromised under Fe stress, lowering cellular carbon and increasing Si:C ratios in particulate matter [*Hoffman et al.*, 2006]. In terms of species composition, low Fe can shift the relative abundance of diatom species and of other taxa that have inherently different elemental compositions [*Marchetti et al.*, 2010; *Durkin et al.*, 2012; *Assmy et al.*, 2013]. Together, these two mechanisms contribute to the lower productivity and reduced nitrate use in high-nitrate low-chlorophyll (HNLC) regions [e.g., *de Baar et al.*, 2005; *Boyd et al.*, 2007].

Because opal is denser than seawater, enhanced diatom silicification under low Fe adds to the ballasting effect of diatom opal on particle export, potentially increasing the gravitational export of organic matter. However, the higher Si:N and Si:C ratios within diatoms under Fe stress reduces the amount of diatom organic matter exported for a given opal flux. The opposing influences of increased ballasting versus higher diatom Si:C and Si:N ratios make it difficult to predict the effect of low Fe on diatom-mediated organic matter export a priori. Here we used a Lagrangian experimental and sampling framework, together with drifting sediment traps, to examine the distribution of Fe, macronutrients, phytoplankton biomass, phytoplankton rate processes, and export along a frontal region located 120 km off the southern California coast. Our results point to the presence of low-Fe waters within a coastal-water cyclone and along the axis of the front, with strong effects on nutrient drawdown ratios, carbon export, and carbon export efficiency.

2. Methods

2.1. Sampling

The P1106 cruise was conducted ~120 km to the southwest of Point Conception, California (Figure 1) aboard the *R/V Melville* from 18 June to 17 July 2011 as part of the California Current Ecosystem (CCE) Long-Term Ecological Research (LTER) program. Lagrangian-style process studies (referred to as "cycles") and two high-resolution spatial transects were conducted at locations relative to a frontal feature whose location was determined by real-time monitoring of the conditions using a Sea Soar and a Moving Vessel Profiler. Similar Lagrangian-style experimental designs have been conducted on previous CCE LTER cruises [e.g., *Landry et al.*, 2009, 2012].

A total of six cycles were conducted targeting three areas: two on the oceanic side of the front, two within the frontal region, and two on the coastal side of the front. For brevity, these three areas will be denoted as oceanic, frontal, and coastal. Each cycle lasted 3 days starting near midnight of day one with the deployment of a surface drifter with a holey-sock drogue at 15 m [e.g., *Stukel et al.*, 2011] and a surface-tethered sediment trap array with VERTEX PIT-style sediment traps at 100 m [*Stukel et al.*, 2013]. CTD hydrocasts for nutrients, phytoplankton biomass, and phytoplankton rate processes were conducted on day one and on day two of each cycle, with day three activity limited to casts for hydrography and stock measurements.

Vertical profiles of Fe distribution were made on days one and two of each cycle using either a trace metal rosette with Teflon-coated 5 L X-Niskin bottles (Ocean Test Equipment) deployed on nonmetallic hydroline (Cycles 1–4) or Teflon-coated 12 L GO-Flo bottles (General Oceanics) mounted directly on the hydroline and tripped via Teflon messengers (Cycles 5 and 6). Sampling depths were determined from the meter readout on the winch for the GO-Flo casts, or based on pressure and triggered by an auto-fire module (Seabird Electronics) mounted on the rosette for the X-Niskin casts. GO-Flo or Niskin casts were performed immediately following a cast by the standard ship CTD rosette, and depths were chosen based on the real-time

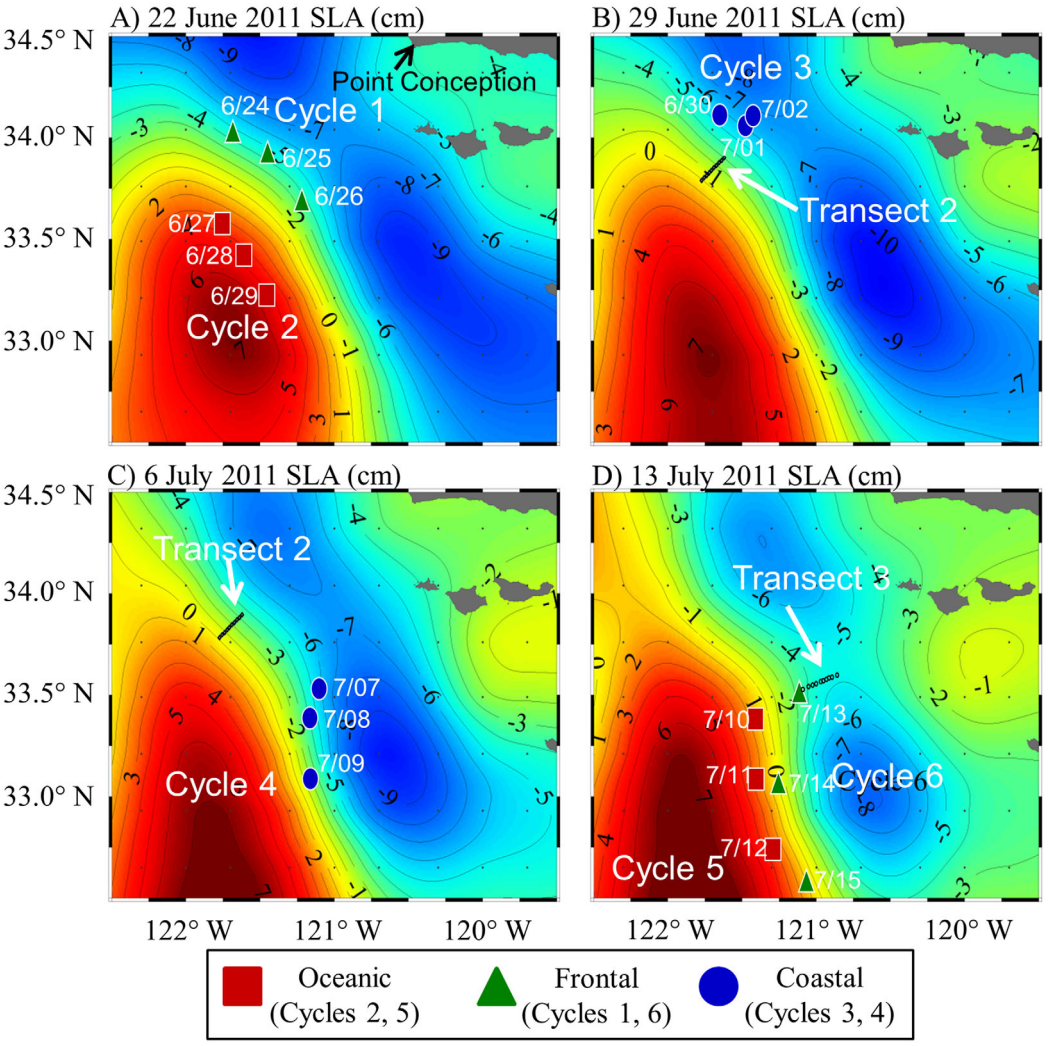

Figure 1. Locations of stations sampled during the P1106 cruise relative to sea-surface-height anomalies (SSHa, in cm, colors and contours). The locations of Transects 2 and 3, and the Lagrangian process Cycles 1–6, are depicted. SSHa fields are for: (a) 22 June, (b) 29 June, (c) 6 July, and (d) 13 July 2011. Dates for each process station are listed (month/day). Symbols represent the different cycle types: oceanic (squares), frontal (triangles), and coastal (circles) or the high-resolution transects (Figures 1b–1d, small circles). Adapted from *Krause et al.* [2015].

hydrographic data from the ship's rosette. GO-Flo or X-Niskin bottles were sampled inside a Class-100 trace metal clean van upon arriving on deck.

CTD/rosette casts involving phytoplankton rate measurements were conducted to depths of 500 m, and Niskin bottles were used to collect water in the upper 40–100 m, depending on euphotic zone depth. For rate process measurements (silica production, primary productivity), incubation bottles were secured to a surface-tethered productivity array in mesh bags and incubated in situ. Each sample was incubated at the same depth from which it was collected. Water sampling, water processing and array deployments were all done prior to sunrise on days one and two. After 24 h, the day one incubated samples from the array were retrieved and day two samples deployed. This same retrieval occurred on day three, followed by recovery of the sediment traps and drogue. Samples for rate assessments were processed immediately upon retrieval, and sediment traps were processed within a few hours.

In addition to the cycles, three high-resolution transects were conducted across the front from local sunset to local sunrise, with 10 planned stations spaced at an interval of 3 km. At each station, a CTD cast was made and water was collected from the upper 85 m. For logistical reasons, only nutrients and standing stock measurements were made on each transect, and no vertical profiles for Fe were taken. The first

transect was aborted part way through the operation. Here we report data from Transects 2 and 3 (Figures 1b–1d).

A 6-day on-deck incubation experiment was performed on the first day of Cycle 3 (Figure 1b) to investigate the relationship between nutrient ratios and Fe stress. The water was collected from 30 m using the trace metal rosette. Water from multiple X-Niskins was homogenized inside the clean van in a conditioned 50 L acid-cleaned carboy prior to subsampling into 4 L trace-metal cleaned polycarbonate bottles. Three bottles were left unamended to serve as controls, and three bottles were augmented with 5 nM $FeCl_3$. All six bottles were sampled daily in a clean van for chlorophyll *a* (Chl *a*), and phytoplankton taxonomy and pigment measurements were made at initial and final time points only. Further details on the incubation experiment setup and results are presented elsewhere [*Bundy*, 2014], but a subset of the data is used here to demonstrate the effects of Fe-limitation on the phytoplankton community.

2.2. Measurements

Seawater nutrient samples were filtered through 0.2 μm capsule filters (Supor Acropak), frozen, and analyzed for NO_3^-, NO_2^-, NH_4^+, and PO_4^{3-} concentrations by autoanalyzer analysis on shore using standard CCE protocols (http://cce.lternet.edu/data/methods-manual), and an additional sample was refrigerated at 4°C until analysis for $Si(OH)_4$ concentration (<4 h) at sea using a sensitive manual colorimetric method [*Brzezinski and Nelson*, 1995]. Chl *a* concentrations were determined by filtering 250 mL of seawater through glass fiber filters (GF/F), extracting in 90% acetone in the dark at −20°C for 24 h, and reading on a Turner 10AU fluorometer while at sea [*Strickland and Parsons*, 1972]. Samples for biogenic silica ($bSiO_2$) concentration were filtered through 0.6 μm polycarbonate filters and analyzed ashore as described by *Krause et al*. [2015]. Samples for particulate organic carbon (POC) were filtered through precombusted GF/F filters and analyzed by Dumas combustion on a CHN Analyzer at the Scripps Institution of Oceanography Analytical Facility.

Rates of primary production were measured using the ^{14}C bicarbonate method [e.g., *Landry et al*., 2010] following CCE LTER protocols (http://cce.lternet.edu/data/methods-manual). Rates of silica production were measured using $^{32}Si(OH)_4$ as described by *Krause et al*. [2015]. Samples from PIT traps were analyzed for $bSiO_2$ and POC concentration as described by *Krause et al*. [2015].

For depth profiles of total dissolved [Fe], seawater subsamples were pressure-filtered (>99% N_2 AirGas) through precleaned 0.2 μm Acropak capsule filters (Acropak 200, VWR International) and immediately acidified to pH 1.8 using Optima grade HCl (2 mL/L, Fisher Scientific) in 250 mL low-density polyethylene (LDPE) bottles. Samples were stored for approximately 2 months and analyzed according to *King and Barbeau* [2011] using flow-injection analysis with chemiluminescent detection. Blanks were determined based on triplicate measurements of three separate blank samples, resulting in a blank of 0.083 ± 0.023 nM (sd, $n = 72$) and a detection limit of 0.070 nM (3 times blank SD). Sampling and analysis of Fe (SAFe) standards [*Johnson et al*., 2007] were run in addition to internal standards, yielding good agreement with reported values (S1: 0.11 ± 0.02 nM, sd, $n = 39$, D2: 0.93 ± 0.07 nM, sd, $n = 36$, GS 0.51 ± 0.02 nM, sd, $n = 12$; http://es.ucsc.edu/~kbruland/GeotracesSaFe/kwbGeotracesSaFe.html).

Phytoplankton pigment concentrations were measured during the on-deck grow-out experiment by collecting 2 L samples and filtering immediately through GF/F filters. Filters were then placed in cryovials and stored in liquid nitrogen until analysis by high-performance liquid chromatography (HPLC) according to *Zapata et al*. [2000]. Phytoplankton cell abundances were measured by collecting 50 mL of unfiltered seawater, preserving with two drops of 10% formaldehyde and enumerating ashore using an inverted microscope using the Utermöhl method [*UNESCO*, 1981; *Utermöhl*, 1958].

Sea surface height anomalies (SSHa) were used to examine the local eddy field. Data were produced by Salto/Duacs and distributed by Aviso (http://www.aviso.oceanobs.com). Data were contoured in Ocean Data View 4.6.2 (Schlitzer, R., Ocean Data View, http://odv.awi.de, 2014).

3. Results

3.1. Physical Context

We adopt the criteria for identifying the frontal region used by *Krause et al*. [2015]. They classified stations in the study region with average mixed-layer salinity of <33.15, 33.15–33.45, and >33.45, as representing

oceanic, frontal, and coastal conditions, respectively. This classification scheme is used to define waters along the high-resolution transects and to categorize the stations occupied during each cycle (Table 1). When this classification scheme is examined relative to sea surface height anomalies (SSHa) (Figure 1), it is seen that the frontal region was a transition zone between an offshore anticyclone and an inshore pair of developing cyclones. The drifter tracks for each cycle indicate strong equatorward flow within the frontal region (Figure 1). Coastal stations were generally associated with the two cyclones and oceanic stations with the anticyclone (Figure 1 and Table 1). Frontal stations varied in their position relative to the gradient in SSHa between the anticyclone and cyclones (Figure 1 and Table 1).

3.2. Nutrient and Biomass Distributions on Transects

The most northern transect across the front, Transect 2, spanned the region between the offshore anticyclone and the northern cyclone (Figures 1b and 1c). The anticyclone was moving south during the cruise (Figure 1), so the position of Transect 2 (conducted 2–3 July) relative to the anticyclone and transition zone is somewhat uncertain. Transect 2 sampled oceanic waters only at its southwest extreme where near-surface silicic acid concentrations were low ($<$1.5 μM) and nitrate was undetectable ($<$0.1 μM) (Figures 2a and 2b). The remainder of the stations sampled on Transect 2 meet the salinity criteria for frontal waters (Figure 2a), consistent with this transect being located largely within the transition zone between eddies (Figure 1b); no coastal waters were sampled. Silicic acid concentrations in frontal surface waters were very low ($<$0.6 μM, Figure 2a) and nitrate concentrations relatively high ($>$5 μM, Figure 2b), especially in the region where horizontal salinity gradients were strongest (4–12 km section distance). Salinities exceeded 33.4, with very low silicic acid to nitrate (Si:N) ratios, $<$0.25, associated with the high-salinity water (Figure 2c). Salinity decreased shoreward, and silicic acid and nitrate concentrations increased to $\sim$1.5 μM and $\sim$3 μM, respectively with Si:N ratios remaining below 0.5 (Figure 2c). Both biogenic silica and Chl *a* concentrations were highest in low Si:N, high-salinity waters (Figures 2d and 2e).

Transect 3 was performed to the southeast of Transect 2 with a similar northeast to southwest orientation (Figure 1d). Transect 3 was occupied 2–3 days after the acquisition of the data for the 13 July SSHa map shown in Figure 1d and is located in the SSHa trough between the two cyclones (Figure 1d). Nutrient concentrations and salinity were considerably higher below 80 m on Transect 3 compared to Transect 2 (Figures 2a and 2f) consistent with isopycnal shoaling beneath the cyclones. Like Transect 2, Transect 3 sampled oceanic waters only at its southwest extreme, but unlike Transect 2 coastal waters with salinities $>$33.5 were well sampled in the northeast. Horizontal salinity gradients within the frontal waters were stronger than on Transect 2, with near vertical isohalines in the upper 40 m (5–10 km along the section, Figure 1). Silicic acid concentrations above the nutricline in frontal waters were low ($\sim$2 μM, Figure 2f) compared to the coastal waters, but nitrate remained high ($\sim$4 μM, Figure 2g) leading to Si:N of $<$0.75 in frontal waters (Figure 2h). In the oceanic waters at the southwestern end of Transect 3, near-surface silicic acid concentrations decreased to between 1 and 2 μM and nitrate declined to undetectable levels ($<$0.1 μM), leading to very high Si:N ratios. In the inshore coastal waters, near-surface nitrate increased to 3 μM and silicic acid was present at concentrations in excess of 4 μM leading to Si:N ratios $>$ 1 (Figure 2h).

Both biogenic silica and Chl *a* concentrations showed that the distribution of phytoplankton biomass along Transect 3 differed from that observed on Transect 2. Frontal waters with low Si:N ($<$0.75) on Transect 3 contained relatively low biomass compared to elevated concentrations of both constituents inshore of the front in waters where Si:N was 1–2 (Figures 2i and 2j). Chl *a* and biogenic silica concentrations in frontal waters were twofold to threefold lower than on Transect 2. Low biomass was also observed offshore in the oceanic water.

3.3. Dynamics as a Function of Si:N

Krause et al. [2015] describe the distributions of biomass, rate processes, and export on cruise P1106 relative to the distribution of frontal, coastal, and oceanic waters. Here we examine the effects of variations in water column Si:N on these same parameters. Each of the 18 station days during the six Lagrangian cycle studies was classified based on the average Si:N value present above the nutricline. Station days were then grouped according to their Si:N ratios based on relationships between diatom nutritional state and elemental composition. Si:N ratios between 1.0 and 2.0 were taken to represent the ratio of nutrient-replete diatoms, values $<$1 to represent an excess of nitrate over silicic acid relative to diatom demand under nutrient-replete conditions, and values of Si:N $>$ 2 to represent waters with an excess of silicic acid over nitrate relative to

Table 1. Depth-Weighted Average Properties Above the Nutricline[a]

Region (Cycle #)	Latitude (°N)	Longitude (°W)	Top of Nutricline (m)	Salinity	$[Si(OH)_4]:[NO_3]$ (mol:mol)	$[NO_3]:[Fe]$ (μmol:nmol)	$[bSiO_2]$ (μmol L^{-1})	[POC] (μmol L^{-1})	Silica Production (μmol L^{-1} d^{-1})	Primary Production (μmol L^{-1} d^{-1})	100 m $bSiO_2$ Export (mmol m^{-2} d^{-1})	100-m POC Export (mmol m^{-2} d^{-1})
Oceanic (Cy2)	33.58	121.77	60	24.36	88	0.25	0.03	3.46	0.003	0.33	0.14 ± 0.02	5.8
Anticyclone	33.42	121.62	40	24.35	78		0.03	3.13	0.003	0.38		
High Si:N	33.22	121.47	40	24.34	60		0.03					
Oceanic (Cy5)	33.38	121.41	35	24.23	≫1000		0.05	6.31	0.004	0.41	0.25 ± 0.03	8.4
Anticyclone	33.08	121.41	43	24.24	133	0.07	0.04	4.61	0.004	0.33		
High Si:N	32.74	121.29	43	24.23	90		0.19	3.78				
Front (Cy1)	34.04	121.70	20	24.75	0.8	26	0.37	7.06	0.11	1.9	5.62 ± 0.39	~
Transition	33.93	121.46	20	24.77	0.8	34	0.35	7.67	0.09	1.7		
Low Si:N	33.70	121.23	20	24.85	0.7		0.44	7.61				
Front (Cy6)	33.52	121.11	18	24.56	0.6	13	0.07	5.98	0.02	1.3	2.01 ± 0.13	20.7
Transition	33.07	121.26	46	24.74	0.7		0.23	9.83	0.06	1.5		
Low Si:N	32.58	121.07	49	24.75	0.9		0.37	7.56				
Coast (Cy3)	34.11	121.65	25	25.11	0.2	21	.0.46	7.23	0.11	2.3	12.09 ± 2.81	7.4
Cyclone	34.06	121.47	25	24.95	0.1	17	0.19	7.95	0.04	2.9		
Low Si:N	34.10	121.42	25	24.87	0.2		0.26	8.53				
Coast (Cy4)	33.53	121.09	10	24.68	0.9[b]	0.5	3.52	37.59	0.10	5.2	3.95 ± 0.19	5.1
Cyclone	33.39	121.16	25	24.72	2.5[b]	0.22	2.38	37.98	0.10	4.5		
Intermediate Si:N	33.09	121.15	8	24.69	1.5[b]		2.21	26.99				
Average		Si:N > 2		33.33 ± 0.04	90 ± 12[c]	0.16 ± 0.04	0.06 ± 0.02	4.3 ± 0.6	0.003 ± 0.000	0.37 ± 0.02	0.19 ± 0.05	7.1 ± 1.3
(±SD)		Si:N = 1–2		33.57 ± 0.00	1.6 ± 0.5	0.38 ± 0.15	2.26 ± 0.41	34 ± 4	0.10 ± 0.00	4.9 ± 0.4	4.0	5.1
		Si:N < 1		32.99 ± 0.02	0.55 ± 0.10	20.0 ± 3.8	0.30 ± 0.04	7.7 ± 0.4	0.07 ± 0.02	1.9 ± 0.2	7.1 ± 5.0	14.0 ± 6.6

[a]Uncertainty terms are standard errors.
[b]Si:N assumed to be in the 0.8–1.5 category for station groupings (see text).
[c]Excludes value of ≫1000 from cycle 5.

diatom demand [*Brzezinski*, 1985]. The one exception to this scheme was Cycle 4. Nitrate and silicic acid had both been depleted to <0.3 μM above the nutricline on each station day within Cycle 4. Given the nearly equal concentration of silicic acid and nitrate in upwelled water along the California Coast [*Zentara and Kamykowski*, 1977], these data imply strong nutrient drawdown within these coastal waters at a Si:N ratio near 1. However, calculated Si:N ratios based on residual nutrient concentrations remaining above the nutricline were between 0.9 and 2.5 (Table 1) because of small variations in low-residual nutrient concentrations. These ratios are ecologically meaningless as the low-residual silicic acid and nitrate concentrations cannot support significant growth or biomass increase. To avoid this artifact, all station days from Cycle 4 are categorized as being in the Si:N = 1–2 category.

Nutrient, Fe, and particle concentrations were examined in surface waters down to the top of the nutricline. The top of the nutricline was defined as one sampling depth shallower than the sampling depth where nutrient concentrations increased by at least 30% relative to the values in the surface layer (concentrations of both nitrate and silicic acid generally varied by <10% and usually <5% above the nutricline). The depth of the nutricline was determined using both silicic acid and nitrate, and its depth at each station was always the same when derived from either nutrient. Depth-averaged properties above the nutricline were calculated by trapezoidal integration to the top of the nutricline followed by normalization to the depth of integration. The station-day grouping resulted in average Si:N mole ratios of 90, 1.6, and 0.55 for the Si:N > 2, Si:N = 1 – 2 and Si:N < 1 categories, respectively (Table 1).

The station-day groupings using the Si:N criteria differ from the oceanic, frontal, and coastal classifications based on salinity (Table 1). The Si:N > 2 category captures all station days from both of the oceanic cycles (Cycles 2 and 5). Si:N of 1–2 includes all station days from coastal Cycle 4 (see above). The low Si:N (<1) stations consist of all stations from frontal Cycles 1 and 6 and all stations from coastal Cycle 3. These cycle groupings formed the basis for all analyses of properties relative to the distribution of Si:N including the rates of export of biogenic silica and of POC (Table 1).

Transect data imply that low Si:N waters should all be located in the front, but this is not the case for cycles. The distribution of Si:N within cycles becomes a coherent pattern when the station locations and dates are viewed in the context of the evolving eddy field (Figure 1). Cycles more closely associated with the

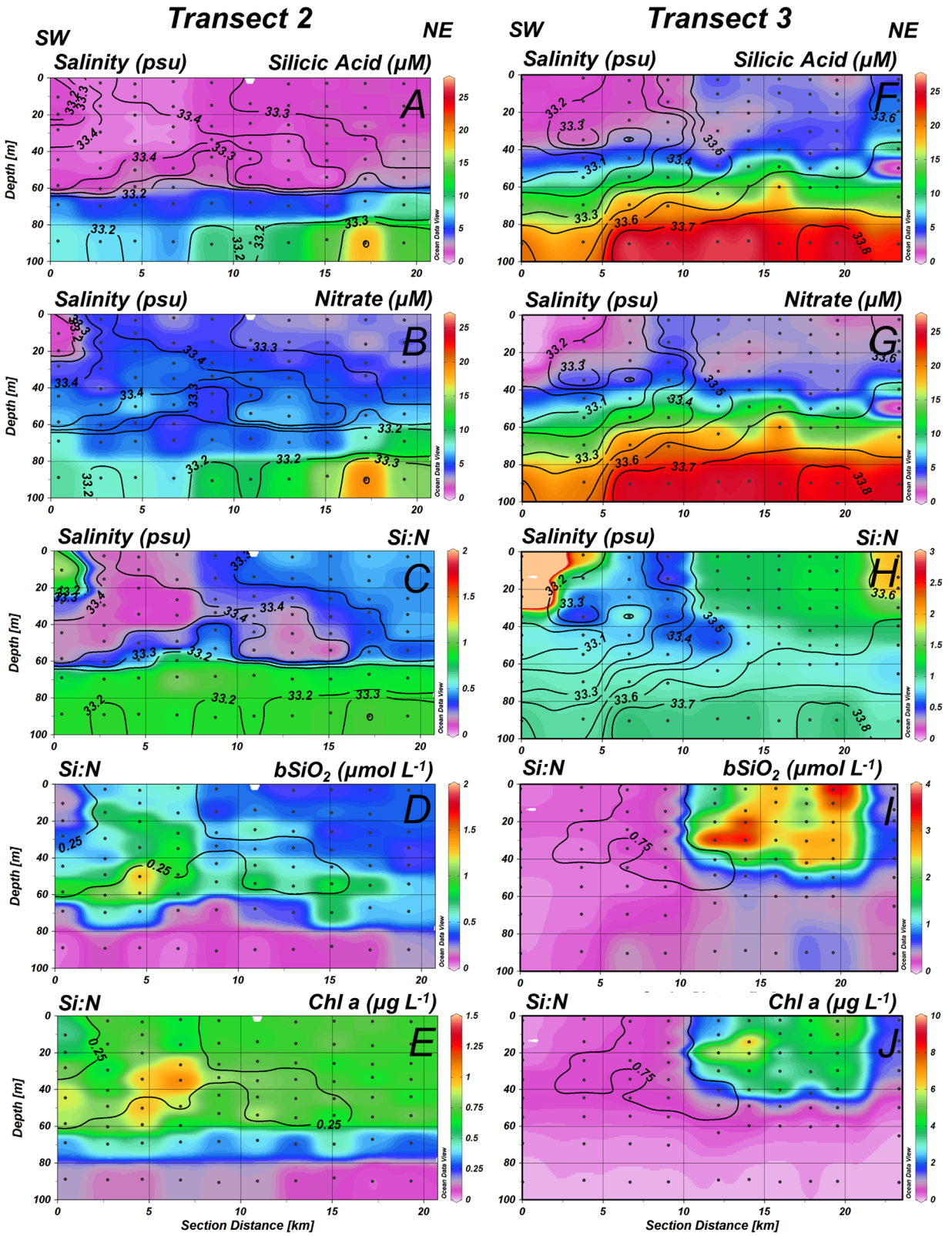

Figure 2. (a–e) Salinity, nutrient concentrations, Si:N ratios, biogenic silica concentrations, and chlorophyll *a* concentrations along Transect 2 and (f–j) Transect 3. Section distance runs from the southwest to the northeast for both transects. Note contours are salinity in Figures 2a–2c and Figures 2f–2h. Contours are Si:N = 0.25 in Figures 2d and 2e and Si:N = 0.75 in Figures 2i and 2j. Transect 2 data adapted from *Krause et al*. [2015].

anticyclone have high Si:N (oceanic Cycles 2 and 5, Figures 1a and 1d). Cycles clearly associated with the northern cyclone (coastal Cycle 3, Figure 1a) have low Si:N. Cycles in the transition zone between the cyclones and anticyclone are more variable with frontal Cycles 1 and 6 showing low Si:N (Figures 1a and 1d) and coastal Cycle 4 showing intermediate Si:N (Figure 1c and Table 1). The precise position of each station relative to the transition zone is somewhat uncertain due the interpolation used to produce the contours of SSHa.

3.4. Indictors of Fe Stress and Response to Added Fe

Low Si:N ratios suggest an influence of Fe stress on diatom growth, which is known to cause the preferential depletion of silicic acid over nitrate off California [e.g., *Bruland et al*., 2001]. We used two approaches to evaluate whether changes in Si:N were related to Fe stress. First, we used the ratio of nitrate to total dissolved Fe as a proxy of Fe stress. *King and Barbeau* [2007] found that N:Fe ratios >12 μM N:1 nM Fe are a strong indicator that phytoplankton nutrient consumption would drive a system to Fe-limitation. Examination of the N:Fe ratios across the three Si:N groupings during the present study show that average N:Fe values exceeded this threshold only for the low Si:N category (Figure 3) such that the Si:N and N:Fe proxies of Fe stress are entirely consistent.

Second, direct evidence of Fe stress in the low Si:N waters was obtained from the on-deck grow-out experiment conducted in waters with Si:N = 0.2 (Cycle 3, station day 1, Table 1) where the addition of 5 nM Fe induced a phytoplankton bloom (Figure 4a). By day 6, diatoms had increased in dominance in both the controls and in the +Fe treatment, but with much greater diatom biomass attained with added Fe. In contrast, coccolithophores, which were initially (T_0) a significant fraction of pigment biomass (Figure 4b), were a small fraction of the pigment biomass in both controls and in the +Fe treatment after 6 days (T_6, Figure 4b). There was not a strong diatom species succession in either the controls or in the +Fe treatments. The initial diatom assemblage was numerically dominated by *Pseudo-nitzschia* spp. (78% of diatom cells), with a 1% contribution by *Chaetoceros* spp. and a mixture of unidentified diatoms comprising the remaining 21%. *Pseudo-nitzschia* spp. remained dominant in both the controls and in the +Fe treatment on day 6, comprising 74% of all diatoms in the +Fe treatment and 61% in the controls, while *Chaetoceros* spp. comprised 1% of diatoms cells in both controls and in the +Fe treatment. Unidentified diatoms increased slightly to 38% in controls and to 25% in the +Fe treatment by day 6.

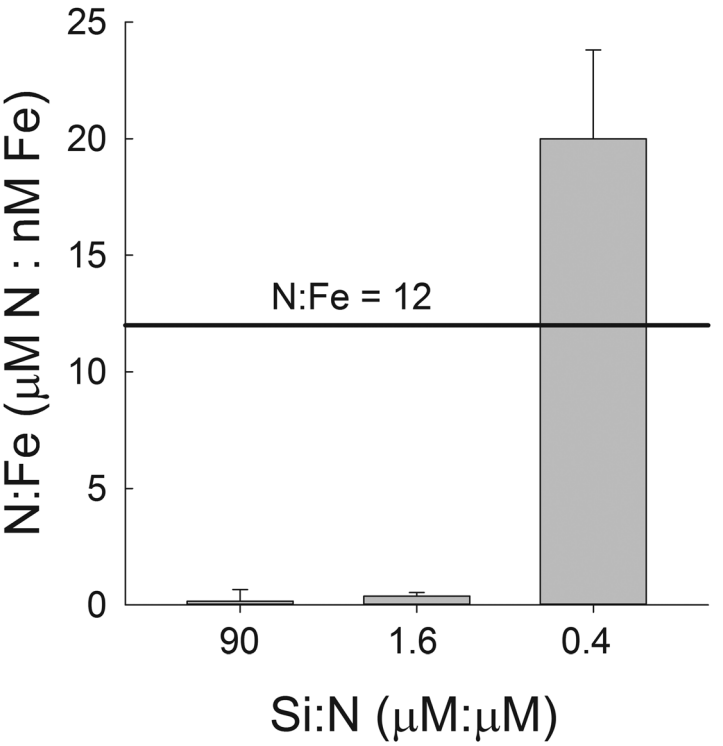

Figure 3. Nitrate to total dissolved iron concentrations (N:Fe, μM:nM) as a function of Si:N. Horizontal line indicates a N:Fe of 12 that is a lower threshold for waters that will become Fe stressed [*King and Barbeau*, 2007]. Error bars are standard errors.

3.5. Nutrient and Biomass Patterns as a Function of Si:N

Si cycling in the upper water column varied significantly with Si:N despite similar average silicic acid concentrations in the mixed layer across Si:N categories; Si:N $>2 = 1.7$ μM $\pm$ 0.2, Si:N 1 – 2 = 0.9 μM $\pm$ 0.3, and Si:N $<1 = 1.7$ μM $\pm$ 0.2 (mean and standard error). Offshore in oceanic waters that dominate the high Si:N category, nutrient concentrations are relatively invariant compared to coastal waters with silicic acid concentrations typically between 1 and 2 μM in this area of the Pacific, while other inorganic macronutrients (N, P) are present at nanomolar levels, leading to the average high Si:N of 90. For the other two Si:N categories,

ambient nutrient concentrations represent a depletion from source waters with a Si:N of about 1.2 [*Zentara and Kamykowski*, 1977]. Thus, where Si:N averaged 1.6, there had been nearly equal depletion of silicic acid and nitrate. In low Si:N waters, silicic acid depletion had exceeded that of nitrate with 4.1 ± 0.8 μM of residual nitrate remaining on average, leading to the low mean Si:N of 0.55.

The average depth-weighted biogenic silica concentrations measured during the cycles were highest for the Si:N = 1.6 group and lowest for the Si:N = 90 group (Figure 5a). Biogenic silica concentrations were also relatively low in the low Si:N waters (Figure 5a). The pattern in average depth-weighted POC concentration as a function of Si:N was similar to that of biogenic silica with relatively low values observed in both high and low Si:N waters, with the highest concentrations present where Si:N averaged 1.6 (Figure 5a).

3.6. Silica Production and Primary Productivity as a Function of Si:N

The depth-weighted average rates of silica production, ρ, and of primary production occurring above the nutricline show that the lowest rates of silica and primary production were measured in the oligotrophic, high Si:N waters (Figure 5). Both rates were highest in waters where Si:N averaged 1.6, with intermediate rates observed for both parameters in low Si:N waters (Figure 5b).

The ratio of silica production to carbon fixation provides insight into the fraction of total carbon fixation by diatoms. Biogenic silica production to organic carbon production ratios were 0.01 ± 0.0, 0.02 ± 0.0, and 0.04 ± 0.00 (std. err.) in the high Si:N, intermediate Si:N, and low Si:N waters, respectively. The average Si:C within nutrient-replete diatoms is 0.13 [*Brzezinski*, 1985]. The low ratios observed across all three Si:N categories suggest considerable primary production by nondiatoms in all cases.

3.7. Biogenic Silica and Particulate Organic Carbon Export as a Function of Si:N

Observations of both low siliceous biomass and low silicic acid concentrations in the low Si:N waters imply that considerable biogenic silica had been exported during the development of the low Si:N condition. Measures of the gravitational export of biogenic silica at 100 m show a high average rate of biogenic silica export beneath low Si:N waters that was 2 and 30 times that observed beneath the intermediate and high Si:N waters, respectively (Figure 5c), although rates were statistically similar in the intermediate and low Si:N categories (Figure 5c). Similar trends were observed for POC export where carbon export was also inversely related to Si:N (Figure 5c). The high rates of carbon export in low Si:N waters are driven in part by the very high POC export during frontal Cycle 6 (Table 1). However, even for coastal Cycle 3, carbon export was comparable to that observed at cycles dominated by intermediate and high Si:N stations, supporting substantial POC export from low Si:N waters (Table 1).

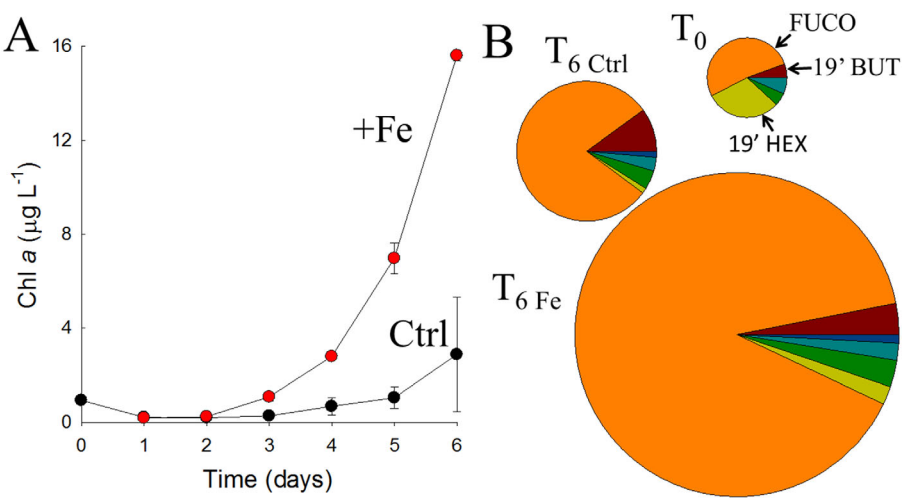

Figure 4. (a) Change in chlorophyll *a* concentration over 6 days in on-deck grow-out experiments in unamended controls and in experimental treatments with added 5 nM Fe. Error bars are standard deviations among triplicate bottles. (b) Changes in the relative proportions of phytoplankton pigments between the beginning (day T_0) and end (day T_6) of the experiment in controls (Ctrl) and in the +Fe treatments. The area of each pie chart is scaled to chlorophyll biomass on day zero and day six shown in Figure 4a. Segments in the pie charts of pigments represent fucoxanthin (orange), 19′-butanoyloxyfucoxanthin (red), chlorophyll *b* (light blue), zeaxanthin (green), and divinyl chlorophyll a (dark blue).

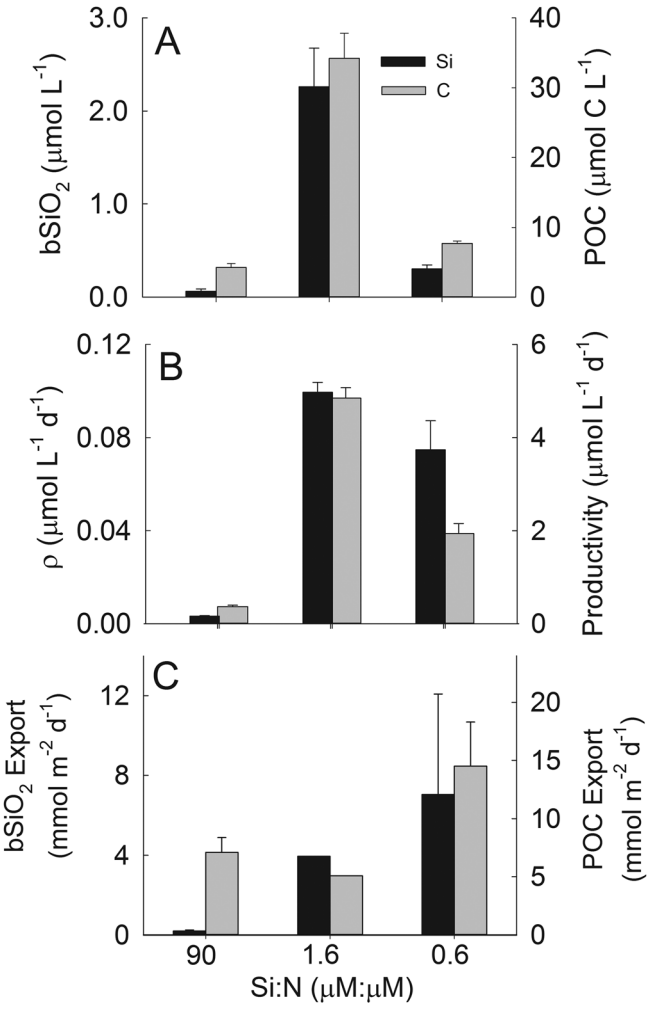

Figure 5. Patterns of average (a) biogenic silica concentration and particulate organic carbon concentration, (b) silica production and primary production, (c) biogenic silica and particulate organic carbon export at 100 m as a function of average Si:N above the nutricline. Error bars are standard errors.

Si:C export ratios were considerably higher than Si:C production ratios in all three Si:N categories (high Si:N = 0.03, intermediate Si:N = 0.78, low Si:N = 0.86). The quotient of the average Si:C of exported particles and the average production rate ratio of silicic acid to inorganic carbon was 3, 38, and 37 for the Si:N > 2, Si:N = 1–2, and Si:N < 1 waters, respectively. These high ratios imply the preferential export of biogenic silica over organic carbon consistent with the operation of a silica pump [*Dugdale et al.*, 1995].

4. Discussion

4.1. Origin of the Low Si:N Waters

The origin of the low Si:N waters encountered during this study is not known. The near vertical isohalines observed during Transect 3 (Figure 2f) drive similar patterns in isopycnals [*Krause et al.*, 2015] indicative of localized vertical mixing, while relatively strong along-front currents in the transition zone between eddies suggest that the low Si:N waters may have been advected a considerable distance. One point of certainty is that the extremely low Si:N ratios could not have arisen from mixing among water masses. Offshore, nitrate was severely depleted relative to silicic acid leading to high Si:N; inshore, silicic acid was generally present at similar or higher concentrations than nitrate. Vertical mixing of deeper waters would introduce deep waters with Si:N ratios of ~1.2. These patterns rule out mixing as mechanism to produce low Si:N waters, which together with the relatively high salinity of the low Si:N waters, support the idea that the nutrient properties within the low Si:N waters evolved during phytoplankton nutrient consumption within previously upwelled waters.

Krause et al. [2015] provide evidence that the two cyclones present during this study differed in their nutrient dynamics. Silicic acid concentrations in the southernmost cyclone were much lower (<0.2 μM) than in the northern cyclone, with strong experimental evidence for severe uptake limitation of Si in the south. The northern cyclone was best sampled during Cycle 3, where the on-deck bottle experiment performed on station day 1 (Figure 4) showed direct evidence of Fe-limitation. The geographic distribution of low Si:N waters in the transition zone suggests southward transport of low Si:N water from the northern cyclone, or beyond, along the axis of the transition zone. Drifter trajectories show strong southerly flow in the transition zone (Figure 1), such that the low Si:N ratios observed during Cycle 6 in the southern portion of the transition zone near the southern cyclone likely originated farther north.

4.2. Indicators of Fe Stress

Significant silicic acid depletion occurs in upwelled waters off California as diatoms typically respond first to upwelling. Because of the excess silicic acid over nitrate in upwelled waters [*Zentara and Kamykowski*, 1977],

diatom growth at a nutrient-replete diatom Si:N ratio of 1 [*Brzezinski*, 1985] would exhaust nitrate before silicic acid. Nitrate use by nondiatoms would enhance this effect. Both of these trends run counter to the production of low Si:N waters. The large deficit of Si observed with residual nitrate of >4 μM in low Si:N waters was more likely the result of the preferential depletion of silicic acid by a pelagic community experiencing Fe stress.

Ample evidence of Fe stress has been found off California, which has been described as a mosaic of Fe-limitation [*Hutchins et al*., 1998]. Waters that upwell from 80 to 120 m depth off California are low in Fe due to a relatively deep ferricline [$\sim$100 m; *King and Barbeau* 2011]. When low-Fe waters upwell near the coast in areas with narrow continental shelves, the waters do not interact strongly with sediments and remain low in Fe [*Bruland et al*., 2001; *Biller and Bruland*, 2014]. Similarly, waters upwelling offshore due to local wind stress curl or to eddy interactions are also isolated from sediments and remain Fe poor [*King and Barbeau*, 2011]. Either mechanism would bring ample silicic acid and nitrate to the surface to support considerable phytoplankton biomass production, but insufficient Fe would eventually drive the system to Fe stress. Both the high N:Fe and low Si:N indices of Fe stress provide complementary evidence that conditions of Fe stress had evolved in frontal and nearby coastal waters, which is also supported by direct experimentation in the grow-out experiment during coastal Cycle 3 (Figure 4).

4.3. Si and Fe Colimitation and Species Effects

Experiments in the eastern equatorial Pacific suggest that Si and Fe can be colimiting factors regulating both nutrient biogeochemistry and diatom species composition [*Marchetti et al*., 2010; *Brzezinski et al*., 2011]. *Brzezinski et al*. [2011] found that silicic acid concentration controlled the rate of silica production in the eastern equatorial Pacific, while Fe-controlled diatom growth rates. A similar situation may be operating off California. In their analysis of CCE Cruise P1106 data, *Krause et al*. [2015] show that additions of silicic acid to low Si:N waters enhanced silica production by nearly a factor of three, while the Fe addition to low Si:N waters in our on-deck grow-out experiment clearly enhanced diatom growth (Figure 4). It may be that Si and Fe colimitation is a common feature in Low-Si High-N Low-Chlorophyll waters.

Studies in the equatorial Pacific [*Marchetti et al*., 2010; *Brzezinski et al*., 2011] and in the subarctic Pacific [*Durkin et al*., 2013] show that relief from Fe stress can induce a diatom species succession. How species composition shifts in response to low Fe contribute to non-Redfield nutrient dynamics is unclear. For example, *Marchetti et al*. [2010] showed the addition of both Si and Fe to low-Fe equatorial waters produced heavily silicified diatoms with low organic matter content. This would imply that, at least in that case, the species effect runs counter to the physiological response to added Fe that results in less-silicified, more organic-rich diatoms. In the Southern Ocean, Fe addition favored diatom taxa with high carbon content (low Si:C) over more heavily silicified forms [*Assmy et al*., 2013]. In the present study, the addition of Fe did not result in a strong shift in diatom species composition in the one experiment conducted in low Si:N waters, despite considerable increase in diatom biomass. It is clear that Fe availability affects both diatom physiology and community structure, but there is considerable unexplained variation in the observed responses.

4.4. Effects on Production and Export

Low Si:N waters had lower rates of both organic carbon and silica production (Figure 5a) and intermediate concentrations of both POC and biogenic silica compared to cycles with average Si:N of 1.6. These patterns together with the high rate of silica export beneath low Si:N waters indicate higher biogenic silica export efficiency in low Si:N waters. Enhanced export of biogenic silica from low Si:N waters is consistent with increased ballasting due to increased diatom biomass and/or increases in frustule thickness under low Fe [*Hutchins and Bruland*, 1998]. Carbon export was also relatively high in the low Si:N waters (Figure 5c), suggesting that increased mineral ballasting also enhanced the export of POC.

Insights into how Fe stress may have affected Si and C export efficiency and the relative contribution of diatoms and nondiatoms to carbon export can be gained by comparing the composition of suspended and exported particles to known shifts in diatom Si:C ratios under low and high Fe conditions. Nutrient-replete diatoms have a cellular Si:C mole ratio of 0.13 [*Brzezinski*, 1985]. That ratio is likely appropriate for the diatoms at stations where Si:N ratios were close to Redfield [Si:N = 1, *Brzezinski*, 1985]. For sites in the Si:N = 1.6 category the Si:C export ratio was 0.78, which is 6 times that expected for intact nutrient-replete diatoms,

implying a large contribution of diatoms to export. Organic matter tends to be remineralized faster than opal, so even in a phytoplankton community consisting of all diatoms, Si:C export ratios would be expected to exceed 0.13. This simple calculation implies a significant fraction of carbon export by diatoms in the intermediate Si:N waters, with a preferential loss of POC over biogenic silica in the upper 100 m.

Diatoms are estimated to be minor contributors to C export in the oligotrophic high Si:N oceanic waters where Si:C of exported particles was 0.03, implying an upper limit to the contribution of diatoms to C export of 23% [(0.03 ÷ 0.13)]. A high contribution of diatoms to C export is estimated for the low Si:N waters where the Si:C export ratio averaged 0.86, which is over 6 times higher than expected for nutrient-replete diatoms. In this case, estimates of carbon export by diatoms must account for the higher diatom Si:C ratios observed under Fe stress. Diatom Si:C ratios increase by a factor of 4–6 under low Fe [*Franck et al*., 2000; *Brzezinski et al*., 2003; *Hoffman et al*., 2006], which is close to the observed Si:C export ratio in low Si:N waters. Under this condition, diatoms are estimated to account for a high fraction of C export, (0.86 ÷ (4 × 0.13) = up to 165%). While these estimates have large uncertainty, they imply that silica ballasting in phytoplankton communities developing under Fe stress have the potential to maintain high carbon export with diatom carbon accounting for a significant fraction of POC export.

The enhanced ballasting of diatoms under low Fe may also enhance the export of nondiatom POC when these particles aggregate with heavily ballasted diatoms. Another factor potentially contributing to the high POC export in low Si:N waters is that Fe stress is not chronic off California. Rather, it evolves as phytoplankton productivity depletes upwelled nutrients. Freshly upwelled waters with high macronutrient:Fe ratios may initially have ample Fe [>0.5 nM Fe; *Biller and Bruland*, 2014] to drive considerable production before decreasing Fe concentrations induce a stress response. Thus, the preferential depletion of silicic acid over nitrate, diatom frustule thickening and other responses to low Fe evolve over time from an initial nutrient-replete state. A temporal evolution of Fe stress may affect organic matter production and diatom silica metabolism differently than would chronic Fe stress, possibly increasing biogenic silica and carbon production and altering export.

4.5. Conceptual Model of the Impacts of Fe

Our results provide insights into how waters with varying N:Fe and Si:N ratios affect diatom productivity and export well offshore of the area of coastal upwelling along California (Figure 1). A conceptual model for how Fe affects diatom nutrient consumption ratios, air-surface CO_2 flux, and export based on our data set is shown in Figure 6. Waters upwelling off California contain high concentrations of both silicic acid and nitrate in a ratio of approximately 1.2 [*Zentara and Kamykowski*, 1977]. Upwelling waters that interact extensively with sediments also contain relatively high concentrations of Fe, compared to those that do not, leading to initially low, or initially high Si:Fe and N:Fe ratios, respectively (Figures 6a and 6b). With both ample Fe and ample macronutrients (Figure 6a), diatom blooms consume nutrients in Redfield proportions resulting in lower total [Fe], the near complete depletion of nitrate, a small pool of residual silicic acid and a strong initial uptake of atmospheric CO_2 (Figure 6c). In contrast, with initially high nitrate and low Fe (Figure 6b), the ensuing bloom is driven to Fe stress, reducing nitrate and carbon consumption compared to silicic acid. The net result is an excess of nitrate over silicic acid, lower initial atmospheric CO_2 uptake, and fewer, more heavily silicified, less organic-rich diatoms (Figure 6d).

Making these scenarios consistent with the evidence for higher export efficiency beneath low Si:N waters (Figure 5) can be achieved by mechanisms that lead to relatively lower POC export efficiency under high Fe (Figure 6c). The thinner frustules produced with ample Fe would enhance POC remineralization by making the less well-armored diatoms more susceptible to grazing and increasing diatom residence times in surface waters through reduced sinking rates. Both factors allow more time for C remineralization and respiration in the upper water column, partially countering the atmospheric CO_2 uptake (Figure 6c). In contrast, the more heavily ballasted diatoms produced under low Fe sink faster and are better armored against grazing [*Smetacek*, 2001; *Hamm et al*., 2003], resulting in proportionately less respiratory losses in plankton communities experiencing low Fe and thus increased POC export efficiency (Figure 6d). The net result is similar DIC use, net atmospheric CO_2 exchange, POC production and carbon export with low and high Fe, but enhanced silica export under low Fe (Figure 6).

4.6. Global Context

Our results have implications for how upwelling Si:N ratios affect nutrient cycling and export in other upwelling-dominated HNLC regions like the Southern Ocean, coastal Peru, or the eastern equatorial Pacific.

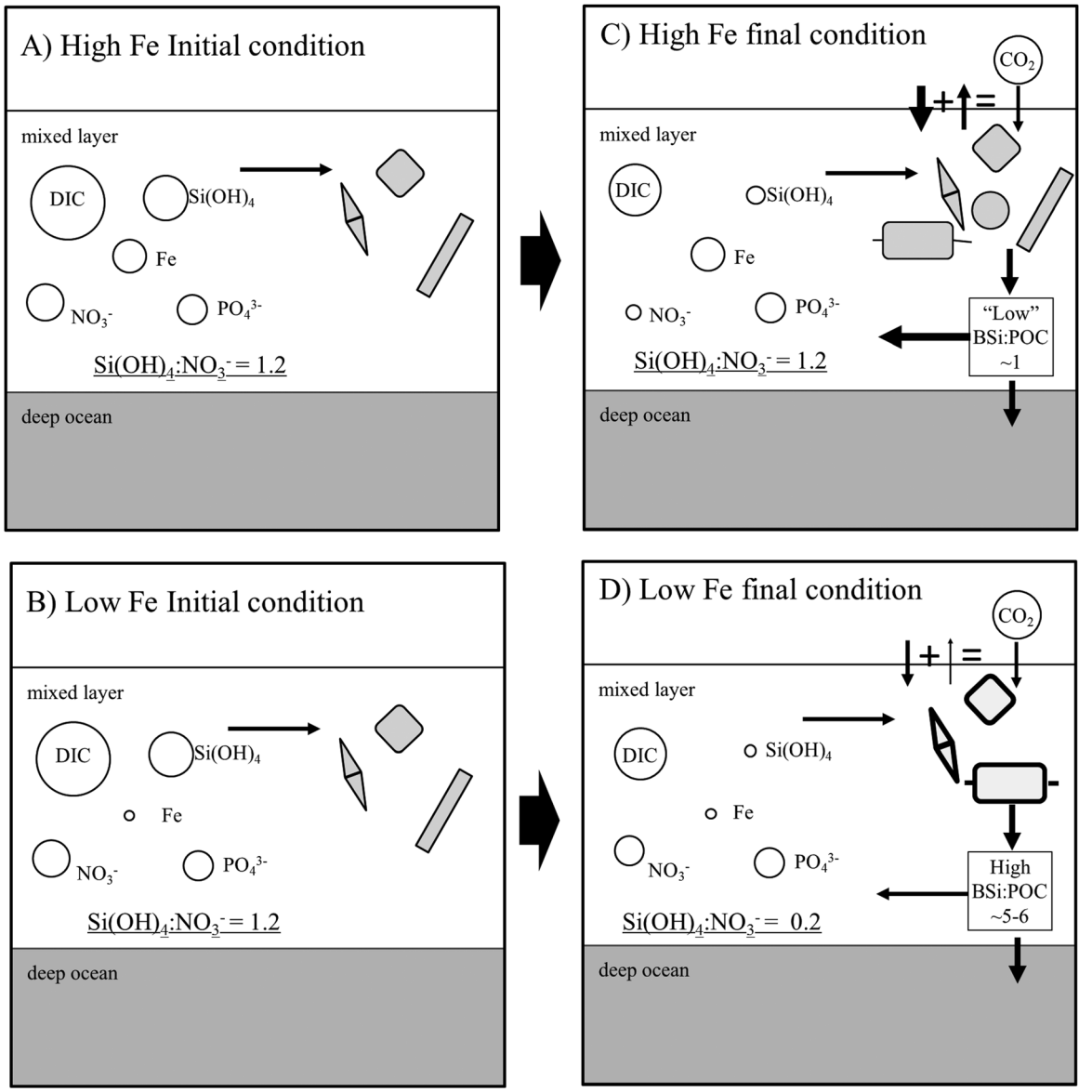

Figure 6. (a and c) Conceptual model of nutrient fluxes, changes in biomass and export when diatoms grow in low N:Fe, high-Fe conditions versus (b and d) with high N:Fe, low Fe that induces Fe-limitation. The size of each circle indicates the relative concentrations of each nutrient. Arrow widths represent the relative magnitudes of fluxes. Internal shading intensity for diatoms represents organic matter content, with lighter shading indicating less. Line thickness around diatoms represents frustule thickness. The arrows leaving the box describing sinking biogenic material represents grazing and other remineralization terms.

In each region, upwelling brings inadequate iron to the surface for phytoplankton to completely utilize upwelled nitrate; however, the Si:N ratio in upwelled waters varies among systems altering how evolving Fe stress affects net opal production and the importance of silica ballasting for export. To first order, the impact of variation in upwelling Si:N can be illustrated mathematically by comparing the ratio of the Si:N in upwelled water, $(Si:N)_{upwelled,}$ to that in diatoms, $(Si:N)_{diatom}$. When $(Si:N)_{upwelled} > (Si:N)_{diatom}$ the system is driven towards nitrate depletion with excess silicic acid remaining. Conversely, when $(Si:N)_{upwelled} < (Si:N)_{diatom}$ silicic acid depletion is favored with excess residual nitrate. Given that $(Si:N)_{diatom}$ varies between 1 and 4 under high and low Fe, respectively, and that $(Si:N)_{upwelled}$ in most HNLC regions is between 1.2 and 2.3, there is an implied switch from nitrate to silicic acid depletion when considering a high versus a low Fe condition. Because calculated silicic acid use is complete under low Fe, and incomplete under high Fe, the fractional increase in net

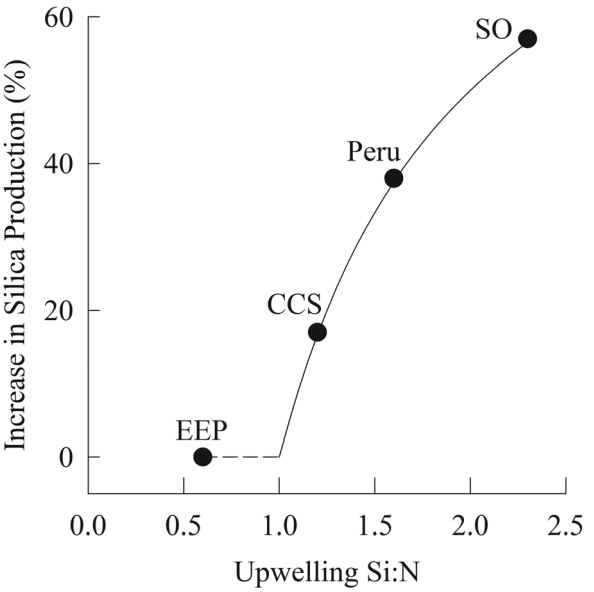

Figure 7. The percent increase in silica production under low Fe conditions compared to high Fe conditions in the Southern Ocean (SO), California Current System (CCS), Peru upwelling, and the eastern equatorial Pacific (EEP) as a function of upwelling silicic acid to nitrate ratio (Si:N). The solid line is that predicted by equation (1). The dashed line connecting the EEP with the solid curve accounts for equation (1) predicting a negative increase in silica production for all values of upwelled Si:N that are less than the Fe-replete diatom Si:N ratio of 1. In these cases, there is sufficient N present to deplete all Si under both low and high Fe and the percent increase in silica production is effectively zero.

silica production between high-Fe and low-Fe states is equal to the fraction of upwelled silicic acid remaining with ample Fe:

$$\left[(\mathrm{Si:N})_{\mathrm{upwelled}} - (\mathrm{Si:N})_{\mathrm{diatom}}\right] \div (\mathrm{Si:N})_{\mathrm{upwelled}} \quad (1)$$

where $(\mathrm{Si:N})_{\mathrm{diatom}} = 1$ reflecting high Fe. Note that actual changes in total net silica production will differ from calculated values if recycled N drives a silica pump [*Dugdale et al*., 1995]. Thus, we view the calculated values as indices, rather than strict measures, of the potential for upwelling Si:N to mediate the diatom silica production and export.

Of all HNLC regions, the Peru coastal upwelling system is most similar to the California Current System (CCS). Both the Peru and CCS systems are eastern boundary currents marked by strong coastal upwelling that exhibit HNLC conditions. Both have intermediate Si:N in upwelling source waters with a value of 1.2 in the CCS [*Zentara and Kamykowski*, 1977] and of 1.6 off Peru [*Dugdale et al*., 1995; *Bruland et al*., 2005]. Like the CCS, waters upwelling over narrow continental shelves off Peru are low in Fe relative to macronutrients leading to the development of low Si:N ratios in surface waters over time [e.g., *Dugdale et al*., 1995; *Hutchins et al*., 2002; *Bruland et al*., 2005]. In both systems, diatoms respond strongly to Fe, but have been observed to become codominant with other taxa off Peru [*Hutchins and Bruland*, 1998; *Hutchins et al*., 2002]. Equation (1) implies that low Fe amplifies total net opal production by only 17% in the CCS and by 38% off Peru (Figure 7). The small increase in production in the CCS suggests that the main effect of low Fe in this system is likely the production of more heavily ballasted, thicker-shelled, diatoms as illustrated by *Hutchins and Bruland* [1998], with increases in total net silica production playing a larger role off Peru.

The oceanic HNLC regions of the Southern Ocean and eastern equatorial Pacific lie at the high and low extremes of upwelling Si:N ratios in HNLC regions, respectively (Figure 7). Si:N upwelling ratio in the Antarctic circumpolar current is 2.3 [e.g., *Pondaven et al*., 2000]. In this case, low Fe increases total net silica production by 57% (Figure 7). Thus, in the Southern Ocean, both nitrate-driven silica production and the potential for silica export each more than double with low Fe, such that shifts in the mass of opal produced with varying Fe may affect export to a greater degree than would frustule thickening. At the opposite extreme is the eastern equatorial Pacific (EEP) where upwelled Si:N is less than the nutrient-replete diatom ratio of 1 with values near 0.6 [*Chai et al*., 2002], and shifts in Fe stress have no effect on potential nitrate-based total net silica production. Ample nitrate exists to support complete silicic acid depletion under both low Fe and high Fe (equation (1) and Figure 7) consistent with Si depletion following Fe addition in the EEP [*Brzezinski et al*., 2011].

4.7. Summary

We have documented that Fe-limitation in waters of the southern California coastal upwelling region can have significant impacts on diatom-mediated carbon export via the silica ballasting effect, as first hypothesized by *Hutchins and Bruland* [1998]. Fe stress produced high Si:N consumption ratios leading to high rates of opal export well offshore of coastal upwelling. Increased silica ballasting in low Si:N waters increased export efficiency facilitating relatively high rates of POC export under low Fe. A future goal is to test the prediction of our conceptual model (Figure 6) that POC export is also modulated by Fe-induced changes in respiratory losses through grazing and POC remineralization in surface waters. Our findings have implications for the role of Fe-

limitation on the global scale in enhancing carbon export via silica ballasting or in enhancing total net silica production in HNLC regimes, depending on the Si:N ratio of upwelled source waters.

Acknowledgments
The primary data for this paper are available through CCE LTER data archive at http://oceaninformatics.ucsd.edu/datazoo/; altimeter products were distributed by Aviso (http://www.aviso.oceanobs.com). We thank the science party and crew of the R/V Melville for their support and technical assistance, specifically A. De Verneil, D. Faber, A. Taylor, and J. Wokuluk; and logistical support at UCSB by J. Jones and L. Windecker. We thank Melissa Carter for cell counts, and T. Fukuda for pigment analyses. This work was supported by the California Current Ecosystem Long Term Ecological Research program under award OCE 1026607 (awarded to M.R.L., R.G., K.B., P.F.) and by the Santa Barbara Coastal Long Term Ecological Research program under awards 9982105 and 0620276, each awarded by the National Science Foundation. We thank Reiner Schlitzer for developing Ocean data View and making it freely available.

References

Assmy, P., et al. (2013), Thick-shelled, grazer-protected diatoms decouple ocean carbon and silicon cycles in the iron-limited Antarctic Circumpolar Current, *Proc. Natl. Acad. Sci. U. S. A.*, *110*, 20,633–20,638.

Biller, D. V., and K. W Bruland (2014), The central California Current transition zone: a broad region exhibiting evidence for iron limitation, *Prog. Oceanogr*, *120*, 370–382, doi:10.1016/j.pocean.2013.11.002.

Boyd, P. W., et al. (2007), Mesoscale iron enrichment experiments 1993–2005: Synthesis and future directions, *Science*, *315*, 612–617.

Bruland, K. W., E. L. Rue, and G. J. Smith (2001), Iron and macronutrients in California coastal upwelling regions: Implications for diatom blooms, *Limnol. Oceanogr.*, *46*, 1661–1674.

Bruland, K. W., E. L. Rue, G. J. Smith, and G. R. DiTullio (2005), Iron, macronutrients and diatom blooms in the Peru upwelling regime: Brown and blue waters of Peru, *Mar. Chem.*, *93*, 81–103.

Brzezinski, M. A. (1985), The Si:C:N ratio of marine diatoms: Interspecific variability and the effect of some environmental variables, *J. Phycol.*, *21*, 347–357.

Brzezinski, M. A., and D. M. Nelson (1995), The annual silica cycle in the Sargasso Sea near Bermuda, *Deep Sea Res., Part I*, *42*, 1215–1237.

Brzezinski, M. A., M.-L. Dickson, D. M. Nelson, and R. Sambrotto (2003), Ratios of Si, C and N Uptake by microplankton in the Southern Ocean, *Deep Sea Res., Part II*, *50*, 619–633.

Brzezinski, M. A., et al. (2011), Co-limitation of diatoms by iron and silicic acid in the equatorial Pacific, *Deep Sea Res., Part II*, *58*, 493–511.

Bundy, R.-M. (2014), Iron and copper organic complexation in marine systems: Detection of multiple ligand classes via electrochemistry, PhD dissertation, 250 pp., Univ. of Calif., San Diego, Calif.

Chai, F., R. C. Dugdale, T. H. Peng, F. P. Wilkerson, and R. T. Barber (2002), One-dimensional ecosystem model of the equatorial Pacific upwelling system. Part I: Model development and silicon and nitrogen cycle, *Deep Sea Res., Part II*, *49*, 2713–2745.

de Baar, H., et al. (2005), Synthesis of iron fertilization experiments: From the Iron Age in the Age of Enlightenment, *J. Geophys. Res.*, *110*, C09S16, doi:10.1029/2004JC002601.

Dugdale, R. C., F. P. Wilkerson, and H. J. Minas (1995), The role of a silicate pump in driving new production, *Deep Sea Res., Part I*, *42*, 697–719.

Durkin, C. A., et al. (2012), Frustule related gene transcription and the influence of diatom commiunity composition on silica precipitation in an iron-limited environment, *Limnol. Oceanogr.*, *57*, 1619–1633.

Durkin, C. A., S. J. Bender, K. Y. K. Chan, K. Gasessner, D. Gunbaum, and E. V. Armbrust (2013), Silicic acid supplied to coastal diatom communities influences cellular silicification and the potential export of carbon, *Limnol. Oceanogr.*, *58*, 1707–1726.

Franck, V. M., M. A. Brzezinski, K. H. Coale, and D. M. Nelson (2000), Iron and silicic acid concentrations regulate Si uptake north and south of the Polar Frontal Zone in the Pacific Sector of the Southern Ocean, *Deep Sea Res., Part II*, *47*, 3315–3338.

Hamm, C. E., R. Merkel, O. Springer, P. Jurkojc, C. Maier, K. Prechtel, and V. Smetacek (2003), Archtitexture and material properties of diatom shells provide effective mechanical protection, *Nature*, *421*, 841–843.

Hoffman, L. J., I. Peeken, K. Lochte, P. Assmy, and M. Veldhuis (2006), Different reactions of Southern Ocean phytoplankton size clases to iron fertilization, *Limnol. Oceanogr.*, *51*, 1217–1229.

Hutchins, D. A., and K. W. Bruland (1998), Iron-limited diatom growth and Si:N uptake ratios in a coastal upwelling regime, *Nature*, *393*, 561–564.

Hutchins, D. A., G. R. DiTullio, Y. Zhang, and K. W. Bruland (1998), An iron limitation mosaic in the California upwelling regime, *Limnol. Oceanogr.*, *43*, 1037–1054.

Hutchins, D. A., et al. (2002), Phytoplankton iron limitation in teh Humbolt Current an Peru Upwelling, *Limnol. Oceanogr.*, *47*, 997–1011.

Johnson, K. S., et al. (2007), Developing standards for dissolved iron in seawater, *Eos, Trans. Am. Geophys. Union*, *88*(11), 131–132.

King, A. L., and K. Barbeau (2007), Evidence for phytoplankton iron limitation in the southern California Current System, *Mar. Ecol. Prog. Ser.*, *342*, 91–103.

King, A. L., and K. A. Barbeau (2011), Dissolved iron and macronutrient distributions in the southern California Current System, *J. Geophys. Res.*, *116*, C03018, doi:10.1029/2010JC006324.

Krause, J. W., M. A. Brzezinski, R. Goericke, M. R. Landry, M. D. Ohman, M. R. Stukel, and A. G. Taylor (2015), Variability in diatom contributions to biomass, organic matter production and export across a frontal gradient in the California Current Ecosystem, *J. Geophys. Res. Oceans*, *120*, 1032–1047, doi:10.1002/2014JC010472.

Landry, M. R., M. D. Ohman, R. Goericke, M. R. Stukel, and K. Tsyrklevich (2009), Lagrangian studies of phytoplankton growth and grazing relationships in a coastal upwelling ecosystem off Southern California, *Prog. Oceanogr.*, *83*, 208–216.

Landry, M. R., K. E. Selph, A. G. Taylor, M. Décima, W. M. Balch, and R. R. Bidigare (2011), Phytoplankton growth, grazing and production balances in the HNLC equatorial Pacific, *Deep Sea Res. II*, *58*, 524–535.

Landry, M. R., et al. (2012) Pelagic community responses to a deep-water front in the California Current Ecosystem: Overview of the A-Front Study, *J. Plankton Res.*, *34*, 739–748.

Marchetti, A., and P. J. Harrison (2007), Coupled changes in the cell morphology and the elemental (C, N and Si) composition of the pennate diatom *Pseudo-nitzschia* due to iron deficiency, *Limnol. Oceanogr.*, *52*, 2270–2284.

Marchetti, A., et al. (2010), Iron and silicic acid effects on phytoplankton productivity, diversity, and chemical composition in the equatorial Pacific Ocean, *Limnol. Oceanogr.*, *55*, 11–29.

Rykaczewski, R. R., and D. M. Checkley (2008), Influence of ocean winds on the pelagic ecosystem in upwelling regions, *Proc. Natl. Acad. Sci. U. S. A.*, *105*, 1965–1970.

Pondaven, P., O. Ragueneau, P. Tréguer, A. Hauvespre, L. Dezileau, and J. L. Reysss (2000), Resolving the "opal paradox" in the Southern Ocean, *Nature*, *405*, 168–172.

Smetacek, V. A. (2001), A watery arms race, *Nature*, *411*, 745.

Strickland, J. D. H., and T. R. Parsons (1972), *A Practical Handbook of Seawater Analysis*, 2nd ed., Fish. Res. Bd. Can., Ottawa.

Stukel, M. R., M. R. Landry, C. R. Benitez-Nelson, and R. Goericke (2011), Trophic cycling and carbon export relationships in the California Current Ecosystem, *Limnol. Oceanogr.*, *56*, 1866–1878.

Stukel, M. R., M. D. Ohman, C. R. Benitez-Nelson, and M. R. Landry (2013), Contributions of mesozooplankton to vertical carbon export in a coastal upwelling system, *Mar. Ecol. Prog. Ser.*, *491*, 47–65.

Takeda, S. (1998), Influence of iron availability on nutrient consumption ratio of diatoms in oceanic waters, *Nature*, *393*, 774–777.

UNESCO (1981), Background papers and supporting data on the Practical Salinity Scale 1978, in *UNESCO Tech. Pap. Mar. Sci.*, *37*, 144 pp., France.

Utermöhl, H. (1958), Zur Vervolkommung der quantitativen phytoplankton, *Mitt. Int. Verein. Limnol.*, *9*, 1–39.

Washburn, L., et al. (1991), Water mass subduction and the transport of phytoplankton in a coastal upwelling system, *J. Geophys. Res.*, *96*, 14,927–14,945.

Zapata, M., F. Rodriguez, and J. L. Garrido (2000), Separation of chlorophylls and carotenoids from marine phytoplankton: A new HPLC method using a reversed phase C8 column and pyridinecontaining mobile phases, *Mar. Ecol. Prog. Ser.*, *195*, 29–45.

Zentara, S.-J., and D. Kamykowski (1977), Latitudinal relationships among temperature and selected plant nutrients along the west coast of North and South America, *J. Mar. Res.*, *35*, 321–337.